

Nonlinear Frequency Shifts due to Phase Coherent Interactions in Incompressible Hall MHD Turbulence

E.C. Hansen,¹ Prerana Sharma,^{1,2} and S.M. Mahajan¹

¹*Institute of Fusion Studies, University of Texas at Austin*

²*Physics Department, Ujjain Engineering College*

(*Electronic mail: ehansen99@utexas.edu)

(Dated: 19 February 2026)

Turbulence in the magnetized plasma is well understood to be the consequence of wave interactions. When the Hall effect is added to the minimum magnetohydrodynamics (MHD), the MHD waves become dispersive and different nonlinear interactions are expected. The emergent turbulent state will thus be expected to be different. For incompressible Hall MHD we develop a reduced model for wave-wave interactions concentrating on those processes that will lead to phase coherent modifications to the linear dispersion of a given wave. We show that these special interactions provide an amplitude-dependent contribution to the linear dispersion relation, which yields nonlinear frequency shifts. The resonance-driven frequency shifts are dominant and add damping or growth to the linear dispersion. The damping/growth rates represent the nonlinear time scales for energy redistribution and can be used in conjunction with a conjecture like the “critical balance” to estimate the energy spectral content.

I. INTRODUCTION

The ability to support waves is one of the primary features that distinguishes magneto plasmas from neutral fluids; it readily translates into different nature of turbulence manifested in the respective models- magnetohydrodynamics (MHD) and hydrodynamics- used to describe them. In MHD, the Alfvén wave connects the oscillating fluctuations in the velocity and magnetic field perturbations.¹ Alfvén waves are a generic name for a host of relatively low frequency (lower than ion cyclotron frequency) wave motions accessible to a magneto-plasma. Due to their essential role in dictating plasma properties, Alfvén waves constitute a highly investigated research area. It is not our intention to survey this vast field but we do give here a list of representative references that the reader may consult. Alfvén waves play a fundamental role in determining the stability of and turbulence in magneto plasmas; they are also an efficient way of heating them.^{2,3} In the solar wind, durable observed correlations between the magnetic and velocity field perturbations reflect Alfvénic activity.^{4,5} A discrete spectrum has been found for Alfvén waves on the inclusion of the parallel electric field in a cylindrical plasma.⁶ The particular manifestations of Alfvén waves in toroidal geometry have also received much attention,^{7,8} and of particular importance has been the destabilization of Alfvén eigenmodes by energetic particles.^{9–12} Many observations of Alfvén eigenmodes in tokamak plasmas and their impact on fast ion confinement and achieving fusion gain have been documented,¹³ and their appearance in optimized stellarators remains an active area of research.^{14,15}

Most of the aforementioned studies deal with the linear wave dynamics of a fluid plasma system. However,

the eventual impact of these waves on the plasma dynamics must be understood in a nonlinear, possibly, turbulent state. The latter, of course, originates in the interactions of these waves.^{16–24} As an example, turbulence in the solar wind exhibits power law spectra according to the relationship of the magnetic and velocity field for the interacting waves.^{25–27}

The goal of many of the cited turbulence theories is the derivation of energy spectrum (often a power law) for an inertial range in which driving mechanisms balance the effects of dissipation. In incompressible magnetohydrodynamics (MHD), for example, Goldreich and Sridhar introduced the critical balance conjecture, which states that the wave spectral content is obtained by balancing the linear oscillation timescale with the nonlinear time scale of wave energy transfer.¹⁹ This assumption, owing to phenomenological arguments, exploits the eddy-damped quasinormal Markovian (EDQNM) closure to calculate a $k_{\perp}^{-5/3}$ spectrum. Another approach to calculation of the spectrum is the Zakharov transformation, which through an assumption of scale invariance in the energy transfer function leads to power law exponents for a stationary spectrum.²⁸ This has been used by Galtier et al. to calculate a k_{\perp}^{-2} spectrum for incompressible MHD,²² and a knee in the incompressible Hall MHD spectrum corresponding to where the Hall effect becomes most important.²³

The spatiotemporal chaos which characterizes turbulence also leads to energy content at a range of frequencies. This may be inferred from the spatial distribution of energy from interactions of eddies of similar and disparate scales, straining and sweeping motions in phase space. In each case, this leads to a power law frequency spectrum.^{29–31} Specifically focusing on the linear waves of the system, simulations of compressible Alfvénic turbulence have found

a Lorentzian frequency spectrum centered about the Alfvén, slow, and fast modes, with broadening caused by the nonlinear wave interactions.³² Where low order resonances are difficult to find in a discrete wavenumber system, the phenomenon of nonlinear broadening allows simulations of resonant interactions because resonances exist within the broadening width.³³ The existence of long time scales of energy transfer is highlighted in the work of Mahajan 2021, which, *inter alia*, constructs a reduced model of Hall MHD turbulence by considering a three-wave subset of the total energy spectrum.²⁴ This is an exactly integrable system for which a timescale of nonlinear energy transfer may be constructed from the Jacobi elliptic function timescale.

The turbulent correction to linear frequencies has been described in generality by Galtier.²⁸ This approach uses the method of two-timing, in which the high frequency of a linear system is corrected by longer period behavior.³⁴ Such an approach eliminates secular perturbative solutions to the van der Pol and Duffing oscillators,³⁵ and is also used by Whitham to analyze nonlinear corrections to a linear dispersion relation for the Klein-Gordon equation.³⁶ This paper explores a different approach to estimate the nonlinear corrections to linear frequency. Using the basic framework developed in Mahajan 2021 (to be called Ma21),²⁴ we will calculate modified frequencies in a weakly turbulent system by choosing from the slew of nonlinear terms only those that are phase coherent with a given mode. These terms nonlinearly modify the linear operator and change the effective frequency via the phase coherent nonlinear terms.

We begin on a similar footing as the multiple scale analysis. We will heavily borrow from Ma21. We begin by reviewing the linear theory and interactions of incompressible Hall MHD in II, concluding with the derivation of the mode coupling coefficients for intra-branch interactions. At this stage, III is devoted to the study of the behavior of these coefficients and in what regions of wavenumber space interactions between waves are strongest. The break from the multiple-scale method comes in IV, where we invoke phase-coherent wave interactions to derive a nonlinear dispersion reflecting the effect of perturbations on the linear frequencies. A calculation for corrections begins in V, where we assume a Maxwellian frequency spectrum for our wave system and use the plasma dispersion function to integrate with a resonant denominator. The final set of integrations over interacting wave numbers is carried out in VI, which allows calculation of the nonlinear frequency shifts.

II. LINEAR THEORY OF INCOMPRESSIBLE HALL MHD

Before calculating of nonlinear frequency shifts, we briefly review the linear waves in an incompressible Hall MHD system immersed in uniform static magnetic field $B_0\hat{z}$. We follow here the approach of Ma21. For an alternative perspective, we refer the interested reader to the work of Galtier in 2006, and Galtier's monograph on MHD in 2016.^{23,24,37}

The perturbed dynamical quantities, the magnetic field \mathbf{b} , and the velocity \mathbf{v} are normalized, respectively to B_0 and the the Alfvén speed $V_A = B_0/(4\pi\rho)^{1/2}$ (with ρ is the constant density). They obey the equations

$$\frac{\partial \mathbf{b}}{\partial t} = \nabla \times \left((\mathbf{v} - (\nabla \times \mathbf{b})) \times (\mathbf{b} + \hat{z}) \right), \quad (1)$$

$$\frac{\partial \mathbf{v}}{\partial t} = \mathcal{P} \left(\mathbf{v} \times (\nabla \times \mathbf{v}) + (\nabla \times \mathbf{b}) \times (\mathbf{b} + \hat{z}) \right), \quad (2)$$

where $\mathcal{P} = \mathcal{I} - \nabla \Delta^{-1} \nabla \cdot$ is a projection operator which reflects the effect of pressure to retain incompressibility.^{38,39} By taking the curl of (2), we work with the vorticity equation

$$\frac{\partial \nabla \times \mathbf{v}}{\partial t} = \nabla \times \left(\mathbf{v} \times (\nabla \times \mathbf{v}) + (\nabla \times \mathbf{b}) \times (\mathbf{b} + \hat{z}) \right). \quad (3)$$

In (1), (2), and (3), time scales are set to the ion cyclotron time scale ω_{ci}^{-1} and length scales to the ion skin depth $d_i = V_A \omega_{ci}^{-1}$.

To derive the linear dispersion, we may readily manipulate the linear system to derive (eliminate \mathbf{v} and using the divergence free conditions),

$$\begin{aligned} \frac{\partial^2 \nabla \times \mathbf{b}}{\partial t^2} &= \frac{\partial}{\partial z} \left(\frac{\partial \nabla \times \mathbf{v}}{\partial t} - \frac{\partial}{\partial t} \nabla \times (\nabla \times \mathbf{b}) \right) \quad (4) \\ &= \frac{\partial^2}{\partial z^2} \nabla \times \mathbf{b} - \frac{\partial}{\partial z} \frac{\partial}{\partial t} \nabla \times (\nabla \times \mathbf{b}) \\ &= \frac{\partial^2}{\partial z^2} \nabla \times \mathbf{b} + \frac{\partial}{\partial z} \frac{\partial}{\partial t} \nabla^2 \mathbf{b}, \end{aligned}$$

that on Fourier decomposition and rearrangement, yields

$$i(k_z^2 - \omega^2) \mathbf{k} \times \mathbf{b} = -k_z \omega k^2 \mathbf{b}, \quad (5)$$

which is the defining equation for a Beltrami field (where the curl of the vector field is aligned with the field). Such a system of circularly polarized waves has been quite extensively studied^{24,40} - the salient results are:

$$\mathbf{b} = b \hat{e}_k, \quad \hat{e}_k = \frac{\mathbf{k} \times \hat{z}}{k_\perp \sqrt{2}} + i \frac{\mathbf{k} \times (\mathbf{k} \times \hat{z})}{k k_\perp \sqrt{2}}, \quad (6)$$

the dispersion relation,

$$\alpha_{k\pm} \equiv \frac{\omega_{\pm}}{k_z} = \frac{k}{2} \pm \sqrt{1 + \frac{k^2}{4}}, \quad (7)$$

and the proportionality of the perturbations

$$\mathbf{v} = -\frac{\mathbf{b}}{\alpha_{k\pm}}. \quad (8)$$

In addition, for the left-handed circularly polarized waves, $i\mathbf{k} \times \hat{e}_k = k\hat{e}_k$.

Notice that the dispersion relation (7) defines two frequency branches for a left-handed circularly polarized wave. We will use the standard nomenclature (Ma21) and refer to α_{k+} as the Alfvén whistler-like branch, and α_{k-} as the Alfvén cyclotron-like branch. Repeating this analysis for the right-handed curl eigenstates, for which $\mathbf{b} \propto \hat{e}_k^\dagger$ and $i\mathbf{k} \times \hat{e}_k^\dagger = -k\hat{e}_k^\dagger$, constructs all normal modes of the incompressible Hall MHD system.

III. HALL MHD COUPLING COEFFICIENTS

Now that we have applied Fourier analysis to the linearized dynamics, we Fourier transform the nonlinear incompressible Hall MHD equations (1) and (3). This leads to convolution integrals which determine the evolution of one Fourier component of the magnetic and velocity field perturbations. To simplify these expressions, we suppose that the interacting magnetic and velocity field fluctuations are excited along the Alfvén whistler-like branch of the left-handed circularly polarized wave; that is,

$$\mathbf{b} = b_k \hat{e}_k \quad \text{and} \quad \mathbf{v} = -\frac{b_k}{\alpha_{k+}} \hat{e}_k. \quad (9)$$

This restricts our analysis to interactions between whistler-like waves in incompressible Hall MHD. However, Ma21 suggests that intra-branch interactions are most relevant for the nonlinear dynamics.²⁴ Along this branch, we find

$$\frac{db_m}{dt} - im_z v_m - im_z |\mathbf{m}| b_m \quad (10)$$

$$= \int d^3 n i \hat{e}_m^\dagger \cdot (\mathbf{m} \times (\hat{e}_n \times \hat{e}_{m-n})) \\ \times \left(\frac{1}{\alpha_{n+}} - |\mathbf{m}| \right) b_n b_{m-n},$$

$$\frac{dv_m}{dt} - im_z b_m \quad (11)$$

$$= \frac{1}{|\mathbf{m}|} \int d^3 n i \hat{e}_m^\dagger \cdot (\mathbf{m} \times (\hat{e}_n \times \hat{e}_{m-n})) \\ \times \left(\frac{|m - n|}{\alpha_{n+} + \alpha_{(m-n)+}} + |n| \right) b_n b_{m-n}.$$

We rewrite the vector product as

$$\hat{e}_m^\dagger \cdot (\mathbf{m} \times (\hat{e}_n \times \hat{e}_{m-n})) \\ = (\mathbf{m} \cdot \hat{e}_{m-n}) \hat{e}_n \cdot \hat{e}_m^\dagger - (\mathbf{m} \cdot \hat{e}_n) \hat{e}_{m-n} \cdot \hat{e}_m^\dagger,$$

which prompts the definition of the interaction kernel of the wavenumbers \mathbf{n} and \mathbf{m} to be the product

$$I_{nm} = (\mathbf{m} \cdot \hat{e}_{m-n})(\hat{e}_n \cdot \hat{e}_m^\dagger). \quad (12)$$

By substituting $n \rightarrow m - n$ in the integral over the other term in the vector product, all of dependence of the interaction on the orientation of \mathbf{n} and \mathbf{m} is accounted for by I_{nm} . The resulting convolution integrals are

$$\int d^3 n i g_{nm} I_{nm} b_n b_{m-n}, \quad (13)$$

$$\int d^3 n i |\mathbf{m}| h_{nm} I_{nm} b_n b_{m-n}, \quad (14)$$

where the coefficients g_{nm} and h_{nm} are defined via

$$g_{nm} = \left(\frac{1}{\alpha_{n+}} - |\mathbf{n}| \right) - \left(\frac{1}{\alpha_{(m-n)+}} - |\mathbf{m} - \mathbf{n}| \right), \quad (15)$$

$$h_{nm} = \left(\frac{1}{\alpha_{n+} + \alpha_{(m-n)+}} - 1 \right) \frac{|\mathbf{m} - \mathbf{n}| - |\mathbf{n}|}{|\mathbf{m}|}. \quad (16)$$

The coefficients $G_{nm} = g_{nm} I_{nm}$ and $H_{nm} = h_{nm} I_{nm}$ calculated above define the energy transfer mechanisms within the Alfvén-whistler branch. To best estimate where interactions are maximized, we analyze these coefficients below. As a summary, we display contours of $J_{nm}^2 = |I_{nm}|^2$, G_{nm}^2 , and H_{nm}^2 in Figure 1 and g_{nm} and h_{nm} in Figure 2. These contours are produced by assuming the wavenumber components parallel to $B_0 \hat{z}$ are small and writing the wavenumber $\mathbf{n} = y \mathbf{m} + x \mathbf{m} \times \hat{z}$.

The interaction kernel appears as a factor determining both G_{nm} and H_{nm} , so we begin by analyzing J_{nm}^2 . This coefficient has a rational function form given by

$$J_{nm}^2 = \frac{|\mathbf{m}|^2}{8} \frac{x^2}{(y-1)^2 + x^2} \left(1 + \frac{y}{\sqrt{y^2 + x^2}} \right)^2. \quad (17)$$

The calculation of this form and other useful identities is presented in Appendix A, and this rational function is displayed in Figure 1a. This function has no irremovable poles (see next paragraph for some discussion of the removable pole at $\mathbf{n} = \mathbf{m}$), and we observe that J_{nm}^2 remains appreciably nonzero for a large range of \mathbf{n} .

Despite this, we comment on zeros and maximum values of J_{nm}^2 . The fact that $x = 0$ forces $J_{nm}^2 = 0$ suggests that when the wavenumber \mathbf{n} is parallel to \mathbf{m} , it does not contribute to its development. This is a result that

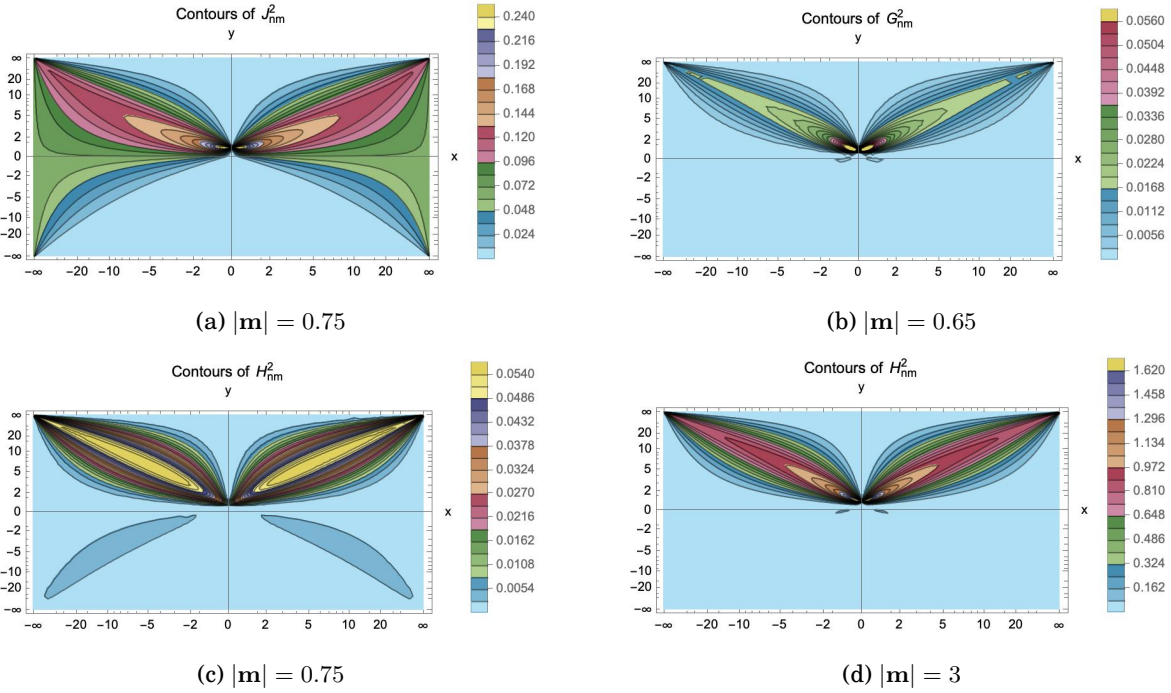


FIG. 1: Contours of coupling coefficients of incompressible Hall MHD as a function of $\mathbf{n} = y \mathbf{m} + x \mathbf{m} \times \hat{z}$.

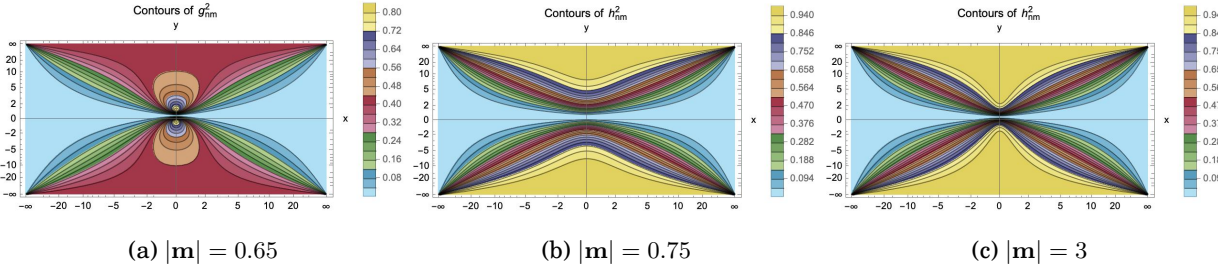


FIG. 2: Contours of g_{nm} and h_{nm} corresponding to Figures 1b, 1c, and 1d, respectively.

has been well established in the literature.^{23,24,40} The second factor $1 + y/\sqrt{x^2 + y^2}$ approaches zero when y is negative and larger than x , which is why the gap in contours is larger around the negative y axis than the positive y axis. However, there are removable singularities in J_{nm}^2 with $\mathbf{n} = \mathbf{m}$. The root of this lies in the fact that a curl eigenstate \hat{e}_m is undefined when $\mathbf{m} = 0$, since at this wavenumber the curl operator is degenerate.

To better understand the functional behavior of J_{nm}^2 , we provide an alternative interpretation of the removable singularities as a non-existent limit of J_{nm}^2 . As described earlier, a limit of J_{nm}^2 as $\mathbf{n} \rightarrow \mathbf{m}$ with \mathbf{n} parallel to \mathbf{m} must be zero. On the other hand, the limit with $y = 1$ as $x \rightarrow 0$ is $|\mathbf{m}|^2/2$, as the factors of x^2 cancel. This limit is the approach of \mathbf{n} to \mathbf{m} with $\mathbf{n} - \mathbf{m}$ perpendicular to \mathbf{m} . In fact, the bounds on the rational functions comprising J_{nm}^2 shows this to be the coefficient's supremum.

Based on the plot of J_{nm}^2 , we see that if we were to pick a wavenumber about which to expand nonlinear interactions, the perpendicular regions to $\mathbf{n} = \mathbf{m}$ appear most interesting. However, the slow decline and asymptote along the upper half plane $y = \pm x$ diagonals suggests that there isn't one particular set of interactions that dominates the nonlinear dynamics.

The coupling coefficients themselves G_{nm} and H_{nm} inherit the strength of J_{nm}^2 along the upper diagonals. Despite this, the coefficients appear to be maximized by different wavenumbers \mathbf{n} . This is a key feature of the coefficients α_{n+} , as the factors of $|\mathbf{m}|$ do not scale out as they do for J_{nm}^2 . We analyze this situation in detail with reference to the prefactor coefficients g_{nm} and h_{nm} , displayed in Figure 2. To ease notation, we refer to α_k in place of α_{k+} . The equation defining α_k is

$$\alpha_k^2 - |\mathbf{k}| \alpha_k - 1 = 0, \quad (18)$$

which implies that $|\mathbf{n}| = \alpha_n - \alpha_n^{-1}$, so we write g_{nm} and h_{nm} exclusively in terms of α_n and α_{m-n} as

$$g_{nm} = -(\alpha_n - \alpha_{m-n})(1 + \frac{2}{\alpha_n \alpha_{m-n}}), \quad (19)$$

$$|\mathbf{m}|h_{nm} = (\alpha_n - \alpha_{m-n})(1 - \frac{1}{\alpha_n^2 \alpha_{m-n}^2}). \quad (20)$$

The common prefactor of $\alpha_n - \alpha_{m-n}$ reflects the antisymmetry used to isolate the interaction kernel in (12). It causes G_{nm} and H_{nm} to both vanish when $y = \frac{1}{2}$.

More interestingly, it offers a unique approach to analyze the behavior of g_{nm} and h_{nm} . Because of the fact that $\mathbf{n} + (\mathbf{m} - \mathbf{n}) = \mathbf{m}$, we can construct an upper bound on $\alpha_n - \alpha_{m-n}$ corresponding to the reverse triangle inequality $||\mathbf{n}| - |\mathbf{m} - \mathbf{n}|| \leq |\mathbf{m}|$. In particular, we find

$$\begin{aligned} & |\alpha_n - \alpha_{m-n} + \alpha_{m-n}^{-1} - \alpha_n^{-1}| \\ &= (1 + \alpha_n^{-1} \alpha_{m-n}^{-1}) |\alpha_n - \alpha_{m-n}| \leq |\mathbf{m}|. \end{aligned} \quad (21)$$

This gives us bounds on g_{nm} and h_{nm}

$$|g_{nm}| \leq \left(1 + \frac{1}{\alpha_n \alpha_{m-n} + 1}\right) |\mathbf{m}|, \quad (22)$$

$$|h_{nm}| \leq \left(1 - \frac{1}{\alpha_n \alpha_{m-n}}\right). \quad (23)$$

We see that the prefactor g_{nm} exceeds its large wavenumber limit $|\mathbf{m}|$ when one of the two vectors \mathbf{n} or $\mathbf{m} - \mathbf{n}$ is small. The magnitude of this maximum, shown near $(0, 0)$ or $(0, 1)$ in 2a, depends on the size of $|\mathbf{m}|$, but the maximum value occurs near the removable singularities of J_{nm} . By contrast, h_{nm} is always less than one, and only reaches this value for large, parallel \mathbf{n} and $\mathbf{m} - \mathbf{n}$. It increases towards one more quickly when $|\mathbf{m}|$ is large so that $1/\alpha_n \alpha_{m-n}$ tends to zero faster, as shown in Figures 2b and 2c. When this increase is fast enough, H_{nm} remains large at $(0, 1)$ and the largest value of H_{nm} also occurs near $(0, 1)$. Otherwise, the product of h_{nm} and J_{nm} is too small close to $\mathbf{n} = \mathbf{m}$, and the value of \mathbf{n} which maximizes H_{nm} occurs deeper into the quadrant as in Figure 1c.

IV. IMPLICIT NONLINEAR DISPERSION RELATION

With the mode coupling coefficients found in the previous section, we are ready to obtain a nonlinear contribution to the dispersion relation. This process begins by obtaining the linear dispersion relation again, but retaining the nonlinear terms. To do this, we assume that all interacting waves are circularly polarized so that $\mathbf{b}_m = b_m \hat{\mathbf{e}}_m$ and $\mathbf{v}_m = v_m \hat{\mathbf{e}}_m$, and we begin from

$$\frac{db_m}{dt} - im_z v_m - im_z |\mathbf{m}| b_m = \int d^3 n i G_{nm} b_n b_{m-n}, \quad (24)$$

$$\frac{dv_m}{dt} - im_z b_m = \int d^3 n i H_{nm} b_n b_{m-n}. \quad (25)$$

Now we can take the time derivative of (24) to eliminate $\frac{dv_m}{dt}$ as before. The result is

$$\begin{aligned} & \frac{d^2 b_m}{dt^2} - im_z |\mathbf{m}| \frac{db}{dt} + m_z^2 b_m \\ &= \int d^3 n i \left(G_{nm} \frac{d}{dt} (b_n b_{m-n}) + im_z H_{nm} b_n b_{m-n} \right). \end{aligned} \quad (26)$$

This is the linear equation we had solved previously for interacting circularly polarized (whistler-branch) waves. We may now find nonlinear effects on the frequency by taking a temporal Fourier transform of this equation. Introducing the symbol $b_{m\omega}$ for $\int b_m(t) e^{-i\omega t} dt$, multiplying by $e^{-i\omega t}$ and integrating yields a nonlinear dispersion relation

$$D_{m\omega} b_{m\omega} \equiv (-\omega^2 + m_z |\mathbf{m}| \omega + m_z^2) b_{m\omega} \quad (27)$$

$$= - \int d^3 n (\omega G_{nm} + m_z H_{nm}) \int d\omega' b_{n\omega'} b_{(m-n)(\omega-\omega')}. \quad (27)$$

Here $D_{m\omega} = -(\omega - m_z \alpha_{m+})(\omega - m_z \alpha_{m-})$ is an abbreviation for the linear dispersion relation of the system.

We want to manipulate this equation such that it is possible to input a spectral and frequency distribution of b_m and return a nonlinear correction to the dispersion relation. To do this, we can use (28) to equally well solve for $b_{n\omega'}$ by writing

$$\begin{aligned} b_{n\omega'} = & -\frac{1}{D_{n\omega'}} \int d^3 n' dq (\omega' G_{n'n} + n_z H_{n'n}) \\ & \times b_{n'q} b_{(n-n')(\omega'-q)}. \end{aligned} \quad (28)$$

In this convolution integral, we have a term containing $b_{m\omega}$ and $b_{(m-n)(\omega'-\omega)}$, which is phase coherent with our original expansion. As a result, this term is expected to contribute much more to the development of $b_{m\omega}$ than the random phases present in other modes. So we approximate

$$b_{n\omega'} = -\frac{\omega' G_{mn} + n_z H_{mn}}{D_{n\omega'}} b_{m\omega} b_{(n-m)(\omega'-\omega)} \quad (29)$$

and the evolution of $b_{m\omega}$ is now given by

$$D_{m\omega} b_{m\omega} = -N_{m\omega} b_{m\omega}, \quad (30)$$

where we have written the nonlinear correction to the linear dispersion relation as $N_{m\omega}$ given by

$$\begin{aligned} & \int d^3 n d\omega' \frac{(\omega G_{nm} + m_z H_{nm})(\omega' G_{mn} + n_z H_{mn})}{(\omega' - n_z \alpha_{n+})(\omega' - n_z \alpha_{n-})} \\ & \times |b_{(m-n)(\omega-\omega')}|^2. \end{aligned} \quad (31)$$

The following sections will evaluate $N_{m\omega}$ in detail to determine the precise form the frequency shifts. Before we proceed with this calculation, we show how to find the shift. We expand the linear frequency as

$\omega = \omega_{m+}(1 + \zeta)$, where ω_{m+} satisfies the linear dispersion relation and ζ is assumed to be $O(E)$, where E is the energy of the magnetic perturbations and should be considered small. Notice that $N_{m\omega}$ contains the perturbed magnetic energy spectrum, so it is $O(E)$. To first order in ζ , this equation then reads

$$-\frac{dD_{m\omega}}{d\omega}|_{\omega_{m+}\omega_{m+}\zeta} = N_{m\omega_{m+}}. \quad (32)$$

The derivative is given by

$$\begin{aligned} -\frac{dD_{m\omega}}{d\omega}|_{\omega_{m+}} &= 2\omega_{m+} - 2|m|m_z \\ &= \frac{2(\omega_{m+}^2 - |m|m_z\omega_{m+})}{\omega_{m+}} = \frac{2m_z}{\alpha_{m+}}, \end{aligned} \quad (33)$$

so our generic formula for the nonlinear frequency shift is

$$\omega_{m+}\zeta = \frac{\alpha_{m+}}{2m_z} N_{m\omega_{m+}}. \quad (34)$$

V. THE FREQUENCY INTEGRAL

The nonlinear correction to the dispersion relation calculated in Section IV may now be evaluated for a particular spectral distribution of $b_{(m-n)(\omega-\omega')}$. This requires an integration over the wavenumbers \mathbf{n} and the frequencies ω' . The dependence of the nonlinear dispersion relation on ω' can be reduced to the integrals over rational functions

$$\begin{aligned} I_{\omega'1} &= \int \frac{\omega' |b_{(m-n)(\omega-\omega')}|^2}{(\omega' - n_z\alpha_{n+})(\omega' - n_z\alpha_{n-})} d\omega', \\ I_{\omega'2} &= \int \frac{|b_{(m-n)(\omega-\omega')}|^2}{(\omega' - n_z\alpha_{n+})(\omega' - n_z\alpha_{n-})} d\omega', \end{aligned} \quad (35)$$

which then yield the nonlinear correction

$$\begin{aligned} N_{m\omega} &= \int d^3n (\omega G_{nm} + m_z H_{nm}) \\ &\quad \times (G_{mn} I_{\omega'1} + n_z H_{mn} I_{\omega'2}). \end{aligned} \quad (36)$$

We must first impose assumptions how the spectrum $|b_{(m-n)(\omega-\omega')}|^2$ depends on $\omega - \omega'$. Given that the many frequencies comprising the spectrum have random phases, we assume that the frequency spectrum is Gaussian distributed,

$$|b_{(m-n)(\omega-\omega')}|^2 = \frac{|b_{m-n}|^2}{\pi\Delta} e^{-(\frac{\omega-\omega'}{\Delta})^2}. \quad (37)$$

Further applying partial fraction decomposition transforms these integrals to

$$I_{\omega'1} = \frac{|b_{m-n}|^2}{\Delta} \int \frac{Ae^{-(\frac{\omega-\omega'}{\Delta})^2}}{\omega' - n_z\alpha_{n+}} - \frac{Be^{-(\frac{\omega-\omega'}{\Delta})^2}}{\omega' - n_z\alpha_{n-}} d\omega', \quad (38)$$

$$I_{\omega'2} = \frac{|b_{m-n}|^2}{\Delta} \int \frac{Ce^{-(\frac{\omega-\omega'}{\Delta})^2}}{\omega' - n_z\alpha_{n+}} - \frac{Ce^{-(\frac{\omega-\omega'}{\Delta})^2}}{\omega' - n_z\alpha_{n-}} d\omega',$$

where the coefficients A , B , and C are given by

$$C = \frac{1}{n_z(\alpha_{n+} - \alpha_{n-})}, A = n_z\alpha_{n+}C, B = n_z\alpha_{n-}C. \quad (39)$$

These frequency integrals closely resemble the plasma dispersion function,⁴¹

$$Z(\xi) = \frac{1}{\sqrt{\pi}} \int dx \frac{e^{-x^2}}{x - \xi}, \quad (40)$$

By making the transformation $\omega' = \omega + \Delta x$, the frequency dependence is fully accounted for as

$$\begin{aligned} \frac{I_{\omega'1}}{|b_{m-n}|^2 \sqrt{\pi}} &= \frac{AZ(\frac{n_z\alpha_{n+}-\omega}{\Delta}) - BZ(\frac{n_z\alpha_{n-}-\omega}{\Delta})}{\Delta}, \\ \frac{I_{\omega'2}}{|b_{m-n}|^2 \sqrt{\pi}} &= \frac{CZ(\frac{n_z\alpha_{n+}-\omega}{\Delta}) - CZ(\frac{n_z\alpha_{n-}-\omega}{\Delta})}{\Delta}. \end{aligned} \quad (41)$$

Before we proceed further, we discuss the limits where the width of the Gaussian distribution Δ is large and small. In the white noise limit where Δ is large, all frequencies are present, and the arguments of the plasma dispersion function are small. Then the plasma dispersion function behaves as⁴¹

$$Z(\xi) = i\sqrt{\pi}e^{-\xi^2} - 2\xi + \frac{4}{3}\xi^3 + \dots, \quad (42)$$

and the imaginary exponential term dominates at order $O(1)$ (representing the contributions of the poles of the frequency integral at $n_z\alpha_{n\pm}$). To leading order, $Z(\xi) = i\sqrt{\pi}$ and the frequency integrals become

$$I_{\omega'1} = i\pi \frac{A - B}{\Delta} |b_{m-n}|^2 = \frac{i\pi |b_{m-n}|^2}{\Delta}, \quad (43)$$

$$I_{\omega'2} = 0, \quad (44)$$

where we used the fact that $A - B = 1$ is an identity from the partial fraction decomposition.

On the other hand, when Δ is small, in general the arguments of the plasma dispersion function are large and we use the asymptotic form⁴¹

$$Z(\xi) = i\sqrt{\pi}e^{-\xi^2} - \frac{1}{\xi} - \frac{1}{2\xi^3} + \dots. \quad (45)$$

With the coming integration over \mathbf{n} , we know that we will find a wavenumber where $\omega' = \omega_{m+}$, picking up the poles from the denominator and requiring the $O(1)$ complex term. Furthermore, if the frequency is narrow enough, $\omega_{m+} - \omega_{m-} \gg \Delta$, and the second plasma dispersion function will disappear. Under that consideration, in this limit the integration becomes

$$I_{\omega'1} = \frac{i\pi A |b_{m-n}|^2}{\Delta} e^{-(n_z\alpha_{n+}-\omega)^2/\Delta^2}, \quad (46)$$

$$I_{\omega'2} = \frac{i\pi C |b_{m-n}|^2}{\Delta} e^{-(n_z\alpha_{n-}-\omega)^2/\Delta^2}.$$

The factor $1/\Delta$ demonstrates that the narrow frequency spectrum can generate a larger impact on the linear frequencies. Yet the fast rate of exponential decay suggests that only \mathbf{n} with $|\mathbf{n}| = |\mathbf{m}|$ contribute to the development of b_m in this regime.

The behavior of the plasma dispersion function suggests that the resonant denominators in our nonlinear dispersion relation cause the linear frequencies to become complex. Consequently, the leading order effect is the growth or dissipation of modes in the Hall MHD system. Had we expanded to higher order in E in Section IV, oscillation frequency shifts would emerge.

VI. EXAMPLE NONLINEAR FREQUENCY CALCULATIONS

In the previous section, we found two limiting forms of nonlinear corrections to the dispersion relation for study of a Gaussian-distributed frequency spectrum. Both cases give priority to the resonant denominator at $m_z \alpha_{m+}$, which recovers the largest contribution to the frequency shift. To summarize, we have found for a wide frequency spectrum

$$N_{m\omega} = \int d^3n (\omega G_{nm} + m_z H_{nm}) G_{mn} \frac{i\pi |b_{m-n}|^2}{\Delta}, \quad (47)$$

and for a narrow spectrum

$$N_{m\omega} = \int d^3n (\omega G_{nm} + m_z H_{nm}) e^{-(n_z \alpha_{n+} - \omega)^2/\Delta^2} \quad (48)$$

$$\times (n_z \alpha_{n+} G_{mn} + n_z H_{mn}) \frac{i\pi C |b_{m-n}|^2}{\Delta}.$$

Now we must finish the calculation of the frequency shift by integrating over wavenumbers.

We begin the integration over wavenumbers by determining what to do with the integration over the small value $m_z - n_z$. In the white noise limit (47), the only dependence on n_z is in its weak contributions to G_{mn} and H_{mn} through $|n|$ and $\alpha_{n\pm}$. As a result, if the spectrum is square-integrable and normalized in n_z , we may trivially integrate.

But there is explicit dependence on n_z in the delta function frequency limit. Since the value of n_z must be small to be consistent with our earlier analysis, we assume the spectrum is a sharply peaked Maxwellian around $m_z - n_z = 0$. This is well approximated by $\delta(m_z - n_z)$, and the integration trivially replaces n_z by m_z .

This enables us to focus the rest of this section on how to evaluate the remaining spatial integrals. We do this for two examples of frequency spectra. Because the narrow frequency spectrum rapidly depletes modes away from the circle $|\mathbf{n}|_\perp = |\mathbf{m}|_\perp$, we begin by considering a spectrum with $\mathbf{m} \approx \mathbf{n}$.

A. $\mathbf{n} \approx \mathbf{m}$

We assume a spectrum in a cylindrical region centered about the mode \mathbf{m} . For the narrow spectrum, Δ is small and the spectrum is taken as

$$b_{m-n}^2 = \begin{cases} b & |\mathbf{m} - \mathbf{n}| < \Delta/m_z \\ 0 & \text{else} \end{cases}.$$

For reference, we note in this case the total magnetic energy of the perturbation near \mathbf{m} is

$$E = \pi(\Delta/m_z)^2 b^2. \quad (49)$$

We carry out the integration for $N_{m\omega_{m+}}$ in Appendix B. The result is

$$N_{m\omega} = -\frac{iE}{\Delta} \frac{1.4 m_z |\mathbf{m}|^2}{2\alpha_{m+}(1+\alpha_{m+}^{-2})} (\alpha_{m+} g_{mm} + h_{mm})^2, \quad (50)$$

which yields a frequency shift

$$-\frac{iE}{\Delta} \frac{1.4}{4} |\mathbf{m}|^2 \frac{(\alpha_{m+} g_{mm} + h_{mm})^2}{(1+1/\alpha_{m+}^2)}. \quad (51)$$

We briefly point out that we can calculate the frequency shift for the large width frequency spectrum for modes close to \mathbf{m} . In this case, Δ is large and the coefficients will vary considerably on that scale, so we must define a separate scale ϵ/m_z for the small region of integration. However, taking similar assumptions leads to the imaginary frequency shift

$$\omega_{m+}\zeta = -\frac{iE}{\Delta} \frac{\pi}{4} |\mathbf{m}|^2 (\alpha_{m+} g_{mm} + h_{mm}) \alpha_{m+} g_{mm}. \quad (52)$$

We display the behavior of these frequency shifts in Figure 3. Despite some differences in their functional form, the corrections appear to have the same power law behavior. As we observed in Section III, in the large $|\mathbf{m}|$ limit, $h_{mm} \rightarrow 1$ where $g_{mm} \rightarrow |\mathbf{m}|$, so this owes to the common factors of $|\mathbf{m}|^2 \alpha_{m+}^2 g_{mm}^2$. Moreover, we notice that the numerical factors preceding the coefficients are similar. As a result, the broad spectrum frequency shift will in practice be much smaller for a comparable energy due to the factor of Δ^{-1} .

This corrective frequency induces an estimate for the nonlinear time scale of energy transfer given by

$$\tau_{nl} = \frac{\Delta}{E} \frac{4/\pi}{|\mathbf{m}|^2 (\alpha_{m+} g_{mm} + h_{mm}) \alpha_{m+} g_{mm}}. \quad (53)$$

Notice that this timescale is inversely proportional to the energy of modes concentrated at \mathbf{m} , as we could expect that a weak nonlinearity takes longer to modify the dynamics of the system. As the magnitude of the wavenumber $|\mathbf{m}|$ increases, the timescale for energy transfer gets smaller and can approach the linear time.

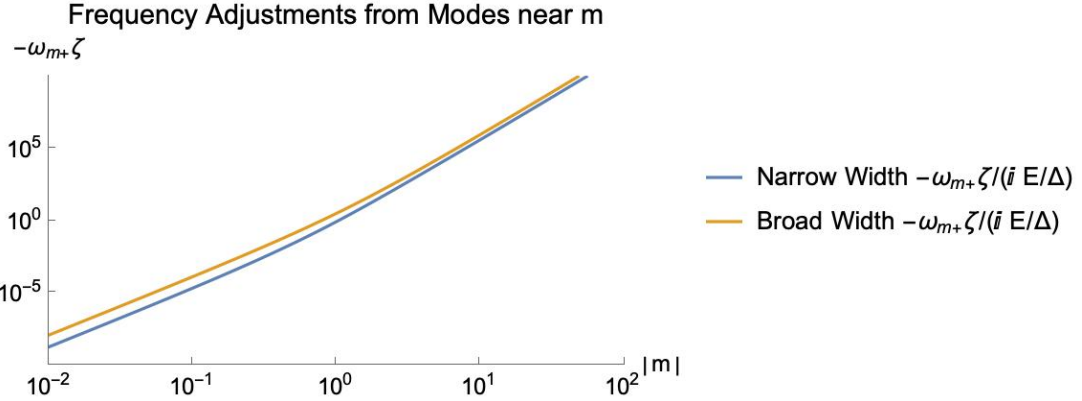


FIG. 3: Frequency shift due to wavenumbers near m . We observe what appears to be power law behavior for $|m|$ large and small, with the frequency shift scaling as $|m|_{\perp}^4$ for small $|m|$ and $|m|_{\perp}^6$ for large $|m|$.

B. Leading Order Broad Spectrum

For the narrow frequency spectrum, the exponential damping from the plasma dispersion function concentrates interactions near the circle $|m|_{\perp} = |n|_{\perp}$. So in this case, we expect interactions with modes near m to dominate the nonlinear dynamics. But the broad frequency spectrum places no such constraints on the nonlinear dynamics. Moreover, the coefficient g_{mn} is qualitatively different from the coefficients g_{nm} and h_{nm} away from the circle $|n| = |m|$. It reflects differences between $|m - n|$ and $|m|$, which are of order $|n|$. This complicates efforts to obtain an expression for the frequency shift in terms of the perturbation energy.

Despite this difficulty, we approach the broad frequency spectrum by integrating the leading order behavior of these coefficients directly. The desired frequency shift is $\frac{\alpha_{m+}}{2m_z} N_m \omega_{m+}$, which for small $|m|$ is given by

$$\frac{i\pi}{2\Delta} \int dn_x dn_y (G_{nm} + H_{nm}) G_{mn} b_{m-n}^2, \quad (54)$$

and for large $|m|$ becomes

$$\frac{i\pi|m|}{2\Delta} \int dn_x dn_y (|m| G_{nm} + H_{nm}) G_{mn} b_{m-n}^2. \quad (55)$$

This requires asymptotic expressions for g_{nm} and h_{nm} , which are summarized in Appendix C. Because of the dependence of g_{nm} and h_{nm} on the norms $|n|$ and $|m - n|$, we find it convenient to use these coordinates for integration. We display the region of integration, set by the triangle inequalities, in Figure 4.

Notice that when g_{nm} and h_{nm} are expanded, we must use as small or large parameters $|n|$ or $|m - n|$. Figure 4 assumes that m is small. In this case, $|n|$ and $|m - n|$ are of similar magnitude (since they differ by at most

$|m|$), so the boundary $\Sigma \equiv |n| + |m - n|$ is used to distinguish when these variables are large and small. When $|m|$ is large, we only consider the case where all three variables $|m|$, $|n|$, and $|m - n|$ are large, so there are no “internal boundaries” used for expansion.

We carry out the integration for the leading order frequency shifts in Appendix D. This is accomplished by transforming into coordinates

$$\Sigma = |n| + |m - n| \quad \text{and} \quad r = \frac{|n| - |m - n|}{|m|}, \quad (56)$$

and exploiting the fact that $|m| < \Sigma$ to estimate the growth rates. The result for large $|m|$ is given by

$$\frac{\pi^2 i}{256\Delta} |m|^5 \int_{|m|}^{\infty} \Sigma^2 b_{m-n}^2 d\Sigma. \quad (57)$$

In these coordinates, the perturbation energy is

$$\frac{\pi}{2} \int_{|m|}^{\infty} \Sigma b_{m-n}^2 d\Sigma \quad (58)$$

so we may interpret the dependence on g_{mn} as relating the frequency shift to the first moment of the energy spectrum. The dependence as $|m|^5$ is consistent with the $|m|^6$ scaling we found for modes near m . (In that case, $\Sigma \approx |m|$.)

The frequency shift for small $|m|$ is given by

$$-\frac{\pi^2 i}{256\Delta} |m|^2 \times \left(\int_2^{\infty} \Sigma^2 b_{m-n}^2 d\Sigma + \frac{3}{4} \int_{|m|}^2 \Sigma^3 b_{m-n}^2 d\Sigma \right),$$

where the contribution from large scales $\Sigma > 2$ is given at left and from large scales $\Sigma < 1$ is given at right. Now we find $|m|^2$ dependence. This is fundamentally

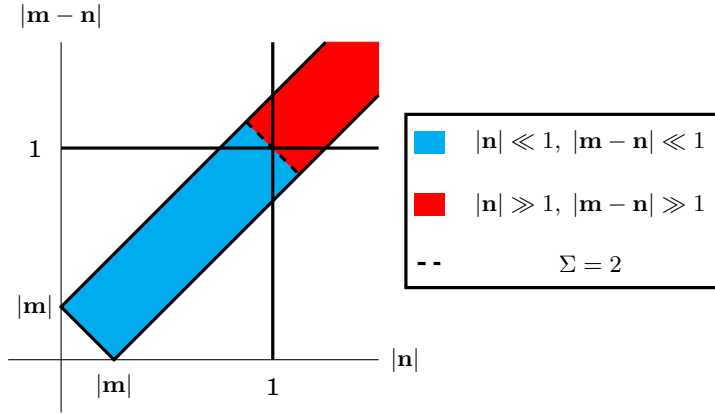


FIG. 4: Integration domain in $|n|$ and $|m - n|$ coordinates for small $|m|$. We show the regions where $|n|$ and $|m - n|$ are considered large and small, corresponding to where $\Sigma \equiv |n| + |m - n| = 2$.

lower order than VI A and owes to the fact that in general h_{nm} is $O(1)$ where h_{mm} is $O(|m|)$. The additional factors of Σ comprising h_{nm} at large scales introduces the second moment of the energy spectrum in the calculation of this frequency shift.

the nonlinear coupling on wavenumber.⁴⁰ This removable singularity is the only place the coupling coefficients are not analytic. The procedure of this paper can be used in a straightforward manner to find frequency corrections due to interactions at any point in wavenumber space.

VII. SUMMARY

Most turbulence problems are essentially unsolvable in entirety. But to gain theoretical understand one always deals with a subset of the total problem. Such theoretical subproblems are rather important in not only advancing our understanding, but also in interpreting simulations that, at least, attempt to do the whole problem. The word nonlinear, in this paper, connotes the subset of nonlinearities that tend to “modify” the linear dispersion relation through nonlinear terms that are phase coherent with the mode under consideration.

The analysis set forth in his paper, therefore, quantifies the modification of frequencies due to this subset of nonlinear interactions in the Hall MHD system. Of particular interest is the investigation of the behavior of the projection of the interaction kernel that reflects the geometric impact of a triadic interaction. Even for this highly simplified nonlinear interaction, the algebra is rather complicated. As no region in wavenumber space strongly sets the interactions, the rational structure of the interaction kernel function complicates the turbulent dynamics.

That a perpendicular approach to the $n = m$ point is the supremum of the interaction kernel, yet a parallel approach is the well-known null interaction found by Waleffe, accentuates the detailed dependence of

The frequency shift we have calculated has direct consequences for the calculation of the energy spectrum. The frequency shifts calculated here come out to be, primarily, damping or growth depending on the wave number - measuring the times for energy exchange and rearrangement in modes. Using the familiar conjecture of critical balance,¹⁹ i.e. by equating the nonlinear time for energy transfer to the linear timescale of the Alfvén wave, we can find the energy spectrum. Such a prescription for the current calculation of Hall MHD will lead to

$$E_m \propto m_z \alpha_m |m|^{-k}. \quad (59)$$

a typical power law shape. Given that $k = 4$ for small $|m|$ and $k = 6$ for large $|m|$, this recovers the known shift in the energy spectrum scaling when length scales pass the ion skin depth.

The analysis of this paper focuses on interactions of the whistler-like branch in Hall MHD. Cyclotron-like branch wave interactions can be recovered by a similar argument, with the transformation $\alpha_{n-} = -\alpha_{n+}^{-1}$ to find maxima of G_{nm} and H_{nm} on this branch. Further exploration of the coupling coefficients via the multiple scale method as in the general work of Galtier would be useful to verify the dependence of frequency corrections on the wavenumber in a general case.²⁸

Appendix A: Reduced Form for Interaction Kernel

In this section, we derive the reduced form of the magnitude of the interaction kernel used in the main text,

$$J_{nm}^2 = \frac{|\mathbf{m}|^2}{8} \frac{x^2}{(y-1)^2 + x^2} \left(1 + \frac{y}{\sqrt{y^2 + x^2}}\right)^2, \quad (\text{A1})$$

where the wavenumber \mathbf{n} is taken to be

$$\mathbf{n} = y \mathbf{m} + x \mathbf{m} \times \hat{z}. \quad (\text{A2})$$

This incorporates the assumption that the field-aligned components of \mathbf{m} and \mathbf{n} are small, which further implies $|\mathbf{m}| \sim |\mathbf{m}|_\perp$.

The two factors comprising the interaction kernel each require a dot product in terms of the circularly polarized vectors \hat{e}_m , \hat{e}_n , and \hat{e}_{m-n} , which have the representation

$$\hat{e}_m = \frac{\mathbf{m} \times \hat{z}}{|\mathbf{m}|_\perp \sqrt{2}} + i \frac{\mathbf{m} \times (\mathbf{m} \times \hat{z})}{|\mathbf{m}| |\mathbf{m}|_\perp \sqrt{2}}. \quad (\text{A3})$$

This form can be exploited to write the circularly polarized vectors in the eigenbasis \mathbf{m} , $\mathbf{m} \times \hat{z}$, $\mathbf{m} \times (\mathbf{m} \times \hat{z})$. Note that

$$(\mathbf{m} \times \hat{z}) \times \hat{z} = m_z \hat{z} - \mathbf{m} \sim -\mathbf{m} \quad (\text{A4})$$

so that $\mathbf{n} \times \hat{z} = y \mathbf{m} \times \hat{z} - x \mathbf{m}$ and the left handed vector corresponding to \mathbf{n} is

$$\begin{aligned} \hat{e}_n &= \frac{\mathbf{n} \times \hat{z}}{|\mathbf{n}|_\perp \sqrt{2}} + i \frac{\mathbf{n} \times (\mathbf{n} \times \hat{z})}{|\mathbf{n}| |\mathbf{n}|_\perp \sqrt{2}} \\ &= \frac{y \mathbf{m} \times \hat{z} - x \mathbf{m}}{|\mathbf{n}|_\perp \sqrt{2}} \\ &\quad + i \frac{(y \mathbf{m} + x \mathbf{m} \times \hat{z}) \times (y \mathbf{m} \times \hat{z} - x \mathbf{m})}{|\mathbf{n}| |\mathbf{n}|_\perp \sqrt{2}} \\ &= \frac{y \mathbf{m} \times \hat{z} - x \mathbf{m}}{|\mathbf{n}|_\perp \sqrt{2}} + i \frac{(x^2 + y^2) \mathbf{m} \times (\mathbf{m} \times \hat{z})}{|\mathbf{n}| |\mathbf{n}|_\perp \sqrt{2}}. \end{aligned} \quad (\text{A5})$$

Given $\mathbf{m} - \mathbf{n} = (1-y) \mathbf{m} - x \mathbf{m} \times \hat{z}$, the substitution $x \rightarrow -x$ and $y \rightarrow (1-y)$ shows that

$$\begin{aligned} \hat{e}_{m-n} &= \frac{(1-y) \mathbf{m} \times \hat{z} + x \mathbf{m}}{|\mathbf{m} - \mathbf{n}|_\perp \sqrt{2}} \\ &\quad + i \frac{(x^2 + (1-y)^2) \mathbf{m} \times (\mathbf{m} \times \hat{z})}{|\mathbf{m} - \mathbf{n}| |\mathbf{m} - \mathbf{n}|_\perp \sqrt{2}}. \end{aligned} \quad (\text{A6})$$

This form allows us to calculate the first factor of the interaction kernel as

$$\mathbf{m} \cdot \hat{e}_{m-n} = \frac{x |\mathbf{m}|^2}{|\mathbf{m} - \mathbf{n}|_\perp \sqrt{2}} \quad (\text{A7})$$

and the second factor as

$$\begin{aligned} \hat{e}_m^\dagger \cdot \hat{e}_n &= \frac{\mathbf{m} \times \hat{z}}{|\mathbf{m}|_\perp \sqrt{2}} \cdot \hat{e}_n - i \frac{\mathbf{m} \times (\mathbf{m} \times \hat{z})}{|\mathbf{m}| |\mathbf{m}|_\perp \sqrt{2}} \cdot \hat{e}_n \\ &= \frac{y |\mathbf{m}|_\perp^2}{2 |\mathbf{m}|_\perp |\mathbf{n}|_\perp} + \frac{(x^2 + y^2) |\mathbf{m} \times (\mathbf{m} \times \hat{z})|^2}{2 |\mathbf{m}| |\mathbf{m}|_\perp |\mathbf{n}| |\mathbf{n}|_\perp}. \end{aligned} \quad (\text{A8})$$

We notice that both factors are purely real, which agrees with previous calculations of the interaction kernel for small m_z and n_z .²⁴ Combining these factors with the result that $|\mathbf{n}|^2 = (y^2 + x^2) |\mathbf{m}|^2$, $|\mathbf{m} - \mathbf{n}|^2 = ((1-y)^2 + x^2) |\mathbf{m}|^2$, and $|\mathbf{m} \times (\mathbf{m} \times \hat{z})| = |\mathbf{m}| |\mathbf{m}|_\perp$, the modulus squared of the interaction kernel is

$$J_{nm}^2 = \frac{|\mathbf{m}|^2}{8} \frac{x^2}{(1-y)^2 + x^2} \left(1 + \frac{y}{\sqrt{x^2 + y^2}}\right)^2. \quad (\text{A9})$$

We also write the interaction kernel in different coordinate systems prepare for the integration of Section (VI). If we take $x = r \sin \theta$ and $y = 1 - r \cos \theta$ to be the scaled coordinates of the vector $\mathbf{m} - \mathbf{n}$, the interaction kernel becomes

$$J_{nm}^2 = \frac{|\mathbf{m}|^2}{8} \sin^2 \theta \left(1 + \frac{1 - r \cos \theta}{\sqrt{1 + r^2 - 2r \cos \theta}}\right)^2. \quad (\text{A10})$$

This form is of interest because the $\sin^2 \theta$ factor reflects the interaction kernel's dependence on the angle of approach of \mathbf{n} to \mathbf{m} . If $\theta = 0$, \mathbf{n} and \mathbf{m} are parallel and there is no interaction. If $\theta = \pi/2$, $\mathbf{m} - \mathbf{n}$ is perpendicular to \mathbf{m} and the interaction is maximized.

It is also possible to use as coordinates the moduli $|\mathbf{n}|$ and $|\mathbf{m} - \mathbf{n}|$. In this system, we have

$$\frac{|\mathbf{n}|^2}{|\mathbf{m}|^2} = x^2 + y^2 \quad \text{and} \quad \frac{|\mathbf{m} - \mathbf{n}|^2}{|\mathbf{m}|^2} = x^2 + (y-1)^2, \quad (\text{A11})$$

so that

$$y = \frac{1}{2} + \frac{|\mathbf{n}|^2 - |\mathbf{m} - \mathbf{n}|^2}{2 |\mathbf{m}|^2} \quad (\text{A12})$$

and $x = \sqrt{(|\mathbf{n}|/|\mathbf{m}|)^2 - y^2}$. Abbreviating $n_y = |\mathbf{m}| y$ leads to the following form of the interaction kernel,

$$J_{nm}^2 = \frac{|\mathbf{m}|^2}{8} \frac{(|\mathbf{n}| - n_y)(|\mathbf{n}| + n_y)^3}{|\mathbf{m} - \mathbf{n}|^2 |\mathbf{n}|^2}. \quad (\text{A13})$$

We conclude this section by writing the reduced form of the interaction kernel in a coordinate independent way. Using the fact that

$$x = \frac{(\mathbf{m} \times \hat{z}) \cdot \mathbf{n}}{|\mathbf{m}|^2} \quad \text{and} \quad y = \frac{\mathbf{m} \cdot \mathbf{n}}{|\mathbf{m}|^2}, \quad (\text{A14})$$

the interaction kernel becomes

$$I_{nm} = \frac{\hat{z} \cdot (\mathbf{n} \times \mathbf{m})}{2\sqrt{2} |\mathbf{m} - \mathbf{n}|} \left(1 + \frac{\mathbf{n} \cdot \mathbf{m}}{|\mathbf{n}| |\mathbf{m}|}\right). \quad (\text{A15})$$

Appendix B: Integration of a Circular Spectrum

Our desired nonlinear component of the dispersion relation $N_{m\omega_{m+}}$ is

$$\frac{i\pi m_z^2 C b^2}{\Delta} \int dn_x dn_y (\alpha_{m+} g_{nm} + h_{nm}) \quad (B1)$$

$$\times I_{nm} I_{mn} (\alpha_{n+} g_{mn} + h_{mn}) e^{-\frac{(\alpha_{n+} - \alpha_{m+})^2}{\Delta^2/m_z^2}}.$$

We are going to integrate using a polar coordinate system with $n_x = |\mathbf{m}|r \sin \theta$ and $n_y = |\mathbf{m}| - |\mathbf{m}|r \cos \theta$. However, we suppose that the region of integration of size Δ is very small, so that the exponential factor has the fastest variation in r and the coefficients α_{n+} , g_{nm} , and h_{nm} may be taken as the constants α_{m+} , g_{mm} , and h_{mm} .

Using the coordinate independent form of the interaction kernel (A15) shows that with small parallel wavenumbers, $I_{mn} = -I_{nm} = -J_{nm}$. Furthermore, the impact of the removable pole of the interaction kernel is fully reflected by the sine function in (A10),

$$J_{nm}^2 = \frac{|\mathbf{m}|^2}{8} \sin^2 \theta \left(1 + \frac{1 - r \cos \theta}{\sqrt{1 + r^2 - 2r \cos \theta}} \right)^2$$

$$\approx \frac{|\mathbf{m}|^2}{2} \sin^2 \theta. \quad (B2)$$

To estimate the exponential term, we approximate

$$\alpha_{n+} - \alpha_{m+} \approx \frac{d\alpha_{m+}}{d|\mathbf{m}|} (|\mathbf{n}| - |\mathbf{m}|)$$

$$= |\mathbf{m}| \frac{d\alpha_{m+}}{d|\mathbf{m}|} (\sqrt{1 - 2r \cos \theta + r^2} - 1)$$

$$\approx -|\mathbf{m}| \frac{d\alpha_{m+}}{d|\mathbf{m}|} r \cos \theta,$$

which brings the exponent to the variables of integration. Through implicit differentiation of

$$\alpha_{m+}^2 - |\mathbf{m}| \alpha_{m+} - 1 = 0$$

we find

$$\frac{d\alpha_m}{d|\mathbf{m}|} = \frac{\alpha_{m+}}{2\alpha_{m+} - |\mathbf{m}|} = \frac{1}{1 + \alpha_{m+}^{-2}}. \quad (B3)$$

This is a slowly varying function that ranges between 1 for large $|\mathbf{m}|$ and 1/2 for small $|\mathbf{m}|$. To make this integration tractable, we assume it is constant and equal to $1/d$.

Rescaling r by $\sqrt{d} \frac{\Delta}{m_z |\mathbf{m}|}$ culminates in the expression for $N_{m\omega_{m+}}$

$$-\frac{i\pi m_z^2 C b^2 |\mathbf{m}|^4}{2\Delta} (\alpha_{m+} g_{mm} + h_{mm})^2 \left(\frac{\Delta}{m_z |\mathbf{m}|} \right)^2 I, \quad (B4)$$

with an integral I which we evaluate numerically

$$I = d \int_0^{1/\sqrt{d}} \int_0^{2\pi} r e^{-r^2 \cos^2 \theta} \sin^2 \theta d\theta dr \quad (B5)$$

$$= \begin{cases} 1.403 & d = 1 \\ 1.480 & d = 2 \end{cases}.$$

Given the similarity in these values, we retain the $d = 1$ value and present the result as

$$N_{m\omega} = -\frac{iE}{\Delta} \frac{1.4m_z |\mathbf{m}|^2}{2\alpha_{m+}(1 + \alpha_{m+}^{-2})} (\alpha_{m+} g_{mm} + h_{mm})^2. \quad (B6)$$

Appendix C: Leading Order Expansion of g_{nm} and h_{nm}

By using the fact that $\alpha_{m+}^{-1} = -\alpha_{m-}$, we write g_{nm} and h_{nm} in the forms

$$g_{nm} = \sqrt{1 + \frac{|\mathbf{n}|^2}{4}} - \frac{3}{2} |\mathbf{n}| - \sqrt{1 + \frac{|\mathbf{m} - \mathbf{n}|^2}{4}} + \frac{3}{2} |\mathbf{m} - \mathbf{n}|,$$

$$h_{nm} = \frac{|\mathbf{m} - \mathbf{n}| - |\mathbf{n}|}{|\mathbf{m}|}$$

$$\times \left(\left(\sqrt{1 + \frac{|\mathbf{n}|^2}{4}} - \frac{|\mathbf{n}|}{2} \right) \left(\sqrt{1 + \frac{|\mathbf{m} - \mathbf{n}|^2}{4}} - \frac{|\mathbf{m} - \mathbf{n}|}{2} \right) - 1 \right).$$

When both $|\mathbf{n}|$ and $|\mathbf{m} - \mathbf{n}|$ are small, the square root terms simplify to one, and at leading order

$$g_{nm} \approx -\frac{3}{2} (|\mathbf{n}| - |\mathbf{m} - \mathbf{n}|), \quad (C1)$$

$$h_{nm} \approx \frac{|\mathbf{m} - \mathbf{n}| - |\mathbf{n}|}{|\mathbf{m}|} \times -\left(\frac{|\mathbf{n}| + |\mathbf{m} - \mathbf{n}|}{2} \right)$$

$$\approx \frac{|\mathbf{n}|^2 - |\mathbf{m} - \mathbf{n}|^2}{2|\mathbf{m}|}.$$

In the opposite limit, $\sqrt{1 + (x/2)^2} \approx x/2$, and

$$g_{nm} \approx -(|\mathbf{n}| - |\mathbf{m} - \mathbf{n}|), \quad (C2)$$

$$h_{nm} \approx \frac{|\mathbf{n}| - |\mathbf{m} - \mathbf{n}|}{|\mathbf{m}|}.$$

Appendix D: General Integration of the Broad Frequency Spectrum

To integrate the broad frequency spectrum, we use the sum and difference coordinates

$$\Sigma = |\mathbf{n}| + |\mathbf{m} - \mathbf{n}| \quad \text{and} \quad r = \frac{|\mathbf{n}| - |\mathbf{m} - \mathbf{n}|}{|\mathbf{m}|}, \quad (D1)$$

which models the domain shown in Figure 4 to the integration bounds $-1 \leq r \leq 1$ and $|\mathbf{m}| \leq \Sigma \leq \infty$. We begin the integration process by rewriting g_{nm} , h_{nm} , and J_{nm}^2 in terms of the sum and difference coordinates.

With the leading order expansions of g_{nm} and h_{nm} carried out in Appendix C, we easily write down

$$g_{nm} = \begin{cases} -\frac{3}{2}r|\mathbf{m}| & |\mathbf{n}|, |\mathbf{m} - \mathbf{n}| \ll 1 \\ -r|\mathbf{m}| & |\mathbf{n}|, |\mathbf{m} - \mathbf{n}| \gg 1 \end{cases}, \quad (\text{D2})$$

$$h_{nm} = \begin{cases} \frac{1}{2}r\Sigma & |\mathbf{n}|, |\mathbf{m} - \mathbf{n}| \ll 1 \\ r & |\mathbf{n}|, |\mathbf{m} - \mathbf{n}| \gg 1 \end{cases}. \quad (\text{D3})$$

Notice that $-1 \leq r \leq 1$ by the triangle inequality, so r is independent of the expansion parameter $|\mathbf{m}|$. As a result, we notice from our leading order forms that h_{nm} is $O(1)$ while g_{nm} is $O(|\mathbf{m}|)$. Since J_{nm}^2 is $O(|\mathbf{m}|^2)$, our general broad spectrum frequency shift returns a small $|\mathbf{m}|$ frequency shift at order $O(|\mathbf{m}|^3)$. This is at lower order than the frequency shift previously calculated in Section VIA. The reason for this is that in that case, $\Sigma = |\mathbf{m}|$ so h_{nm} was also $O(|\mathbf{m}|)$.

In general, we expect that g_{mn} will be related to the difference between $|\mathbf{m} - \mathbf{n}|$ and $|\mathbf{m}|$, which is of order $O(|\mathbf{n}|)$. A similar expansion for g_{mn} reveals that

$$g_{mn} = \begin{cases} \frac{3}{4}\Sigma(1 - (r+2)\frac{|\mathbf{m}|}{\Sigma}) & |\mathbf{m}|, |\mathbf{m} - \mathbf{n}|, |\mathbf{n}| \ll 1, \\ \frac{1}{2}\Sigma(1 - (r+3)\frac{|\mathbf{m}|}{\Sigma}) & |\mathbf{m}| \ll 1, |\mathbf{m} - \mathbf{n}|, |\mathbf{n}| \gg 1, \\ \frac{1}{2}\Sigma(1 - (r+2)\frac{|\mathbf{m}|}{\Sigma}) & |\mathbf{m}|, |\mathbf{m} - \mathbf{n}|, |\mathbf{n}| \gg 1, \end{cases}$$

where we include the separate case where $|\mathbf{m}| \ll 1$ and $|\mathbf{n}|, |\mathbf{m} - \mathbf{n}| \gg 1$. (We also neglect the small region where $|\mathbf{m} - \mathbf{n}| \ll 1$ but $|\mathbf{m}|, |\mathbf{n}| \gg 1$).

Progressing with the calculation, we note that

$$\begin{aligned} 2|\mathbf{n}| &= \Sigma + |\mathbf{m}|r, \\ 2|\mathbf{m} - \mathbf{n}| &= \Sigma - |\mathbf{m}|r, \\ 2n_y &= \Sigma r + |\mathbf{m}|, \\ 2(|\mathbf{n}| \pm n_y) &= (1 \pm r)(\Sigma \pm |\mathbf{m}|), \end{aligned} \quad (\text{D4})$$

and substituting this transformation into the interaction kernel (A13) yields

$$\begin{aligned} J_{nm}^2 &= \frac{|\mathbf{m}|^2}{8}(1-r)(1+r)^3 \\ &\times \frac{(1-|\mathbf{m}|/\Sigma)(1+|\mathbf{m}|/\Sigma)^3}{(1-|\mathbf{m}|^2r^2/\Sigma^2)^2}. \end{aligned} \quad (\text{D5})$$

Our last step before integrating is the computation of the Jacobian for the transformation to sum and difference coordinates. The matrix of partial derivatives with respect to n_x and n_y is

$$\begin{bmatrix} \frac{n_x}{|\mathbf{n}|} + \frac{n_x}{|\mathbf{m}-\mathbf{n}|} & \frac{n_y}{|\mathbf{n}|} + \frac{n_y - |\mathbf{m}|}{|\mathbf{m}-\mathbf{n}|} \\ \frac{1}{|\mathbf{m}|}(\frac{n_x}{|\mathbf{n}|} - \frac{n_x}{|\mathbf{m}-\mathbf{n}|}) & \frac{1}{|\mathbf{m}|}(\frac{n_y}{|\mathbf{n}|} - \frac{n_y - |\mathbf{m}|}{|\mathbf{m}-\mathbf{n}|}) \end{bmatrix}. \quad (\text{D6})$$

In calculation of the determinant, only the terms multiplying $\frac{|\mathbf{m}|}{|\mathbf{m}-\mathbf{n}|}$ do not cancel, and the result is

$$\mathcal{J}^{-1} = \frac{2n_x}{|\mathbf{n}||\mathbf{m} - \mathbf{n}|}. \quad (\text{D7})$$

Using the identities above simplifies the result to

$$\mathcal{J}^{-1} = \frac{2\sqrt{(1+r)(1-r)(1-|\mathbf{m}|^2/\Sigma^2)}}{\Sigma(1-|\mathbf{m}|^2r^2/\Sigma^2)}. \quad (\text{D8})$$

To carry out the integration and achieve our main result, we simplify our expressions by assuming that $|\mathbf{m}|/\Sigma \ll 1$. This is justified because $|\mathbf{m}| < \Sigma$ in any case, and inaccuracies are only appreciable within a few multiples of $|\mathbf{m}|$. Such an assumption also reduces the wavenumber dependence of the energy spectrum to dependence on Σ .

Now we are prepared to integrate leading order contributions. For large $|\mathbf{m}|$, the frequency shift is given by

$$-\frac{i\pi|\mathbf{m}|}{2\Delta} \int dn_x dn_y |\mathbf{m}| g_{nm} g_{mn} J_{nm}^2 b_{m-n}^2 \quad (\text{D9})$$

where we have discarded the h_{nm} contribution because it is $O(1)$ while the g_{nm} contribution is $O(|\mathbf{m}|)$. The simplification above leads to the frequency shift

$$\frac{i\pi|\mathbf{m}|^5}{64\Delta} \int_{|\mathbf{m}|}^{\infty} d\Sigma \Sigma^2 b_{m-n}^2 \int_{-1}^1 dr \frac{r(1-r)(r+1)^3}{\sqrt{1-r^2}}. \quad (\text{D10})$$

We evaluate the integration over r as

$$\int_{-1}^1 \frac{r(1-r)(1+r)^3}{(1+r)^{0.5}(1-r)^{0.5}} dr = \frac{\pi}{4}, \quad (\text{D11})$$

simplifying the large $|\mathbf{m}|$ frequency shift to

$$\frac{\pi^2 i}{256\Delta} |\mathbf{m}|^5 \int_{|\mathbf{m}|}^{\infty} \Sigma^2 b_{m-n}^2 d\Sigma. \quad (\text{D12})$$

For the small $|\mathbf{m}|$ integration, we follow Figure 4 by splitting the domain for $\Sigma > 2$ and $\Sigma < 1$, corresponding to where the variables $|\mathbf{n}|$ and $|\mathbf{m} - \mathbf{n}|$ are large and small. We also retain the h_{nm} contribution instead of g_{nm} for small $|\mathbf{m}|$. The contribution to the frequency shift in the small scale region $\Sigma > 2$ is given by

$$-\frac{i\pi}{2\Delta} \int dn_x dn_y h_{nm} g_{mn} J_{nm}^2 b_{m-n}^2. \quad (\text{D13})$$

We notice on substitution, to this order in our asymptotics, that the only differences between this calculation and the large $|\mathbf{m}|$ case are the absent factors of

$-|\mathbf{m}|$ from g_{nm} and the prefactors $|\mathbf{m}|^2$. So the contribution to the frequency shift from small scales for small $|\mathbf{m}|$ is

$$-\frac{\pi^2 i}{256\Delta} |\mathbf{m}|^2 \int_2^\infty \Sigma^2 b_{m-n}^2 d\Sigma. \quad (\text{D14})$$

In the large scale $\Sigma < 1$ regime, we find additional factors of $3/2$ in g_{mn} and $\Sigma/2$ in h_{nm} . As a result, we write down the contribution to the frequency shift as

$$-\frac{3\pi^2 i}{1024\Delta} |\mathbf{m}|^2 \int_{|\mathbf{m}|}^2 \Sigma^3 b_{m-n}^2 d\Sigma. \quad (\text{D15})$$

For reference, the total perturbation energy given by integration over sum and difference coordinates is

$$\begin{aligned} E &= \int_{|\mathbf{m}|}^\infty d\Sigma \int_{-1}^1 dr \frac{\Sigma}{2\sqrt{1-r^2}} b_{m-n} \\ &= \frac{\pi}{2} \int_{|\mathbf{m}|}^\infty \Sigma b_{m-n}^2 d\Sigma. \end{aligned} \quad (\text{D16})$$

ACKNOWLEDGMENTS

This work was supported by U.S. Department of Energy Grant No. DE-FG02-04ER-54742.

- ¹H. Alfvén. Existence of electromagnetic-hydrodynamic waves. *Nature*, 150(3805):405–406, 10 1942.
- ²D. W. Ross, G. L. Chen, and S. M. Mahajan. Kinetic description of Alfvén wave heating. *The Physics of Fluids*, 25(4):652–667, 04 1982.
- ³R. White, L. Chen, and Z. Lin. Resonant plasma heating below the cyclotron frequency. *Physics of Plasmas*, 9(5):1890–1897, 05 2002.
- ⁴J. W. Belcher and L. Davis Jr. Large-amplitude Alfvén waves in the interplanetary medium, 2. *Journal of Geophysical Research (1896-1977)*, 76(16):3534–3563, 1971.
- ⁵K. G. Klein, G. G. Howes, J. M. TenBarge, S. D. Bale, C. H. K. Chen, and C. S. Salem. Using synthetic spacecraft data to interpret compressible fluctuations in solar wind turbulence. *The Astrophysical Journal*, 755(2):159, aug 2012.
- ⁶S. M. Mahajan. Kinetic theory of shear Alfvén waves. *The Physics of Fluids*, 27(9):2238–2247, 09 1984.
- ⁷H. Ye, Z. Sedlacek, and S. M. Mahajan. Two-dimensional analytic theory for toroidal Alfvén eigenmodes. *Physics of Fluids B: Plasma Physics*, 5(8):2999–3011, 08 1993.
- ⁸R. R. Mett and S. M. Mahajan. Kinetic theory of toroidicity-induced Alfvén eigenmodes. *Physics of Fluids B: Plasma Physics*, 4(9):2885–2893, 09 1992.
- ⁹Y. M. Li, S. M. Mahajan, and D. W. Ross. Destabilization of global Alfvén eigenmodes and kinetic Alfvén waves by alpha particles in a tokamak plasma. *The Physics of Fluids*, 30(5):1466–1484, 05 1987.
- ¹⁰L. Chen and F. Zonca. Theory of shear Alfvén waves in toroidal plasmas. *Physica scripta*, 1995:81–90, 1995.
- ¹¹G. Vlad, F. Zonca, and S. Briguglio. Dynamics of Alfvén waves in tokamaks. *La Rivista del Nuovo Cimento*, 22(7):1–97, jul 1999.
- ¹²W. W. Heidbrink. Basic physics of Alfvén instabilities driven by energetic particles in toroidally confined plasmara. *Physics of Plasmas*, 15(5):055501, 02 2008.
- ¹³K.-L. Wong. A review of Alfvén eigenmode observations in toroidal plasmas. *Plasma Physics and Controlled Fusion*, 41(1):R1, jan 1999.
- ¹⁴Y. I. Kolesnichenko, V. V. Lutsenko, H. Wobig, Y. V. Yakovenko, and O. P. Fesenyuk. Alfvén continuum and high-frequency eigenmodes in optimized stellarators. *Physics of Plasmas*, 8(2):491–509, 02 2001.
- ¹⁵E. J. Paul, A. Hyder, E. Rodríguez, R. Jorge, and A. Knyazev. The shear Alfvén continuum of quasisymmetric stellarators. *Journal of Plasma Physics*, 91(4):E101, 2025.
- ¹⁶P. S. Iroshnikov. Turbulence of a Conducting Fluid in a Strong Magnetic Field. *Soviet Astronomy*, 7:566, 2 1964.
- ¹⁷R. H. Kraichnan. Inertial-range spectrum of hydromagnetic turbulence. *The Physics of Fluids*, 8(7):1385–1387, 07 1965.
- ¹⁸S. Sridhar and P. Goldreich. Toward a theory of interstellar turbulence. 1: Weak Alfvénic turbulence. *The Astrophysical Journal*, 432(2):612–621, 1994.
- ¹⁹P. Goldreich and S. Sridhar. Toward a Theory of Interstellar Turbulence. II. Strong Alfvénic Turbulence. *The Astrophysical Journal*, 438:763, 1995.
- ²⁰C. S. Ng and A. Bhattacharjee. Interaction of shear-alfven wave packets: Implication for weak magnetohydrodynamic turbulence in astrophysical plasmas. *The Astrophysical Journal*, 465:845–854, 1996.
- ²¹P. Goldreich and S. Sridhar. Magnetohydrodynamic turbulence revisited. *The Astrophysical journal*, 485(2):680–688, 1997.
- ²²S. Galtier, S. V. Nazarenko, A. C. Newell, and A. Pouquet. A weak turbulence theory for incompressible magnetohydrodynamics. *Journal of Plasma Physics*, 63(5):447–488, 2000.
- ²³S. Galtier. Wave turbulence in incompressible Hall magnetohydrodynamics. *Journal of Plasma Physics*, 72(5):721–769, 2006.
- ²⁴S. M. Mahajan. A new and alternative look at nonlinear Alfvénic states. *Physics of Plasmas*, 28(8):082303, 08 2021.
- ²⁵V. Krishan and S. M. Mahajan. Modeling of short scale turbulence in the solar wind. *Nonlinear Processes in Geophysics*, 12(1):75–81, 2005.
- ²⁶V. Krishan and S. M. Mahajan. Hall-MHD turbulence in the solar atmosphere. *Solar Physics*, 220(1):29–41, 03 2004.
- ²⁷H. M. Abdelhamid, M. Lingam, and S. M. Mahajan. Extended MHD turbulence and its applications to the solar wind. *The Astrophysical Journal*, 829(2):87, sep 2016.
- ²⁸S. Galtier. *Physics of Wave Turbulence*. Cambridge University Press, 2022.
- ²⁹H. Tennekes. Eulerian and Lagrangian time microscales in isotropic turbulence. *Journal of Fluid Mechanics*, 67(3):561–567, 1975.
- ³⁰S. Chen and R. H. Kraichnan. Sweeping decorrelation in isotropic turbulence. *Physics of Fluids A: Fluid Dynamics*, 1(12):2019–2024, 12 1989.
- ³¹Y. Zhou, W. H. Matthaeus, and P. Dmitruk. Colloquium: Magnetohydrodynamic turbulence and time scales in astrophysical and space plasmas. *Rev. Mod. Phys.*, 76:1015–1035, Dec 2004.
- ³²K. H. Yuen, H. Li, and H. Yan. Temporal properties of compressible magnetohydrodynamic turbulence. *The Astrophysical Journal*, 986(2):221, 6 2025.
- ³³C. Connaughton, S. Nazarenko, and A. Pushkarev. Discreteness and quasiresonances in weak turbulence of capillary waves. *Phys. Rev. E*, 63:046306, Mar 2001.
- ³⁴C. M. Bender and S. A. Orszag. *Advanced mathematical methods for scientists and engineers*. Springer, New York, 1999.
- ³⁵S. H. Strogatz. *Nonlinear dynamics and chaos : with applications to physics, biology, chemistry, and engineering*. Westview Press, a member of the Perseus Books Group, Boulder, CO, second edition. edition, 2015.
- ³⁶G. B. Whitham. *Linear and nonlinear waves*. Pure and applied mathematics (John Wiley & Sons). Wiley, New York, 1974.
- ³⁷S. Galtier. *Introduction to Modern Magnetohydrodynamics*. Cambridge University Press, 2022.

bridge University Press, 2016.

³⁸H. A. Rose and P. L. Sulem. Fully developed turbulence and statistical mechanics. *Journal de Physique*, 39(5):441–484, 1978.

³⁹C. Chandre, L. de Guillebon, A. Back, E. Tassi, and P. J. Morrison. On the use of projectors for Hamiltonian systems and their relationship with Dirac brackets. *Journal of Physics A: Mathematical and Theoretical*, 46(12), 2013.

⁴⁰F. Waleffe. The nature of triad interactions in homogeneous turbulence. *Physics of Fluids A: Fluid Dynamics*, 4(2):350–363, 02 1992.

⁴¹B. D. Fried and S. D. Conte. *The plasma dispersion function; the Hilbert transform of the Gaussian*. Academic Press, New York, 1961.

⁴²M. J. Lighthill. Studies on magneto-hydrodynamic waves and other anisotropic wave motions. *Philosophical Transactions of the Royal Society of London. Series A, Mathematical and Physical Sciences*, 252(1014):397–430, 1960.

⁴³E. G. Zweibel and M. Yamada. Magnetic reconnection in astrophysical and laboratory plasmas. *Annual Review of Astronomy and Astrophysics*, 47(Volume 47, 2009):291–332, 2009.

⁴⁴F. Porcelli. Collisionless m=1 tearing mode. *Phys. Rev. Lett.*, 66:425–428, Jan 1991.

⁴⁵R. Fitzpatrick. Scaling of forced magnetic reconnection in the Hall-magnetohydrodynamical Taylor problem with arbitrary guide field. *Physics of Plasmas*, 11(8):3961–3968, 08 2004.

⁴⁶B. Coppi. “Inertial” instabilities in plasmas. *Physics Letters*, 11(3):226–228, 1964.

⁴⁷S. M. Mahajan, P. Sharma, and M. Lingam. Hall MHD waves: A fundamental departure from their mhd counterparts. *Physics of Plasmas*, 31(9):090701, 09 2024.

⁴⁸A. Mesa Dame, H. Qin, E. Palmerduca, and Y. Fu. Wave topology in Hall magnetohydrodynamics. *Phys. Rev. E*, 112:045216, Oct 2025.

⁴⁹H. Goedbloed, R. Keppens, and S. Poedts. *Magnetohydrodynamics of Laboratory and Astrophysical Plasmas*. Cambridge University Press, Cambridge, 1 edition, 2019.